Chapter

Doping and Transfer of High Mobility Graphene Bilayers for Room Temperature Mid-Wave Infrared Photodetectors

Ashok K. Sood, John W. Zeller, Parminder Ghuman, Sachidananda Babu, Nibir K. Dhar, Randy N. Jacobs, Latika S. Chaudhary, Harry Efstathiadis, Samiran Ganguly, Avik W. Ghosh, Sheikh Ziauddin Ahmed and Farjana Ferdous Tonni

Abstract

High-performance graphene-HgCdTe detector technology has been developed combining the best properties of both materials for mid-wave infrared (MWIR) detection and imaging. The graphene functions as a high mobility channel that whisks away carriers before they can recombine, further contributing to detection performance. Comprehensive modeling on the HgCdTe, graphene, and the HgCdTe-graphene interface has aided the design and development of this MWIR detector technology. Chemical doping of the bilayer graphene lattice has enabled *p*-type doping levels in graphene for high mobility implementation in high-performance MWIR HgCdTe detectors. Characterization techniques, including SIMS and XPS, confirm high boron doping concentrations. A spin-on doping (SOD) procedure is outlined that has provided a means of doping layers of graphene on native substrates, while subsequently allowing integration of the doped graphene layers with HgCdTe for final implementation in the MWIR photodetection devices. Successful integration of graphene into HgCdTe photodetectors can thus provide higher MWIR detector efficiency and performance compared to HgCdTe-only detectors. New earth observation measurement capabilities are further enabled by the room temperature operational capability of the graphene-enhanced HgCdTe detectors and arrays to benefit and advance space and terrestrial applications.

Keywords: graphene, HgCdTe, photodetectors, MWIR, mobility, doping, transfer

1. Introduction

1.1 Graphene overview

The term *graphene* is a combination of two words—*graphite* and *alkene*. Graphene denotes a two-dimensional (2-D) sheet of graphite of atomic-scale

thickness resulting due to intercalation of graphite compounds [1, 2]. Graphene can be divided into three different classifications based on the extent of its layer structure, which are monolayer, bilayer, and multilayer graphene, with the latter designating graphene structures consisting of three or more layers [3].

Graphite, another well-known compound of carbon, basically consists of stacked sheets of graphene held in place by van der Waals forces. A third relatively recently discovered carbon compound that has likewise been envisioned as a catalyst essentially comprises rolled-up sheets of graphene commonly known as *carbon nanotubes*. As thus comprising the basic building block of these key carbon materials of varying dimensionalities, graphene has come to be considered the "mother" of graphitic compounds [4].

Chemically speaking, graphene comprises a two-dimensional hexagonal benzene ring-like structure consisting of sp^2-bonded carbon, packed into honeycomb lattice as shown in **Figure 1**, where the C–C bond length is 0.142 nm. It is one of the first 2-D materials known to be stable at room temperature, and in ambient conditions is crystalline and chemically inert. Although stronger than diamond, graphene yet remains as flexible as rubber [6].

From an electrical standpoint, the valence and conduction bands in the band structure of graphene meet at the corners of the Brillouin zone or Dirac points. The consequence of this is that apart from the influence of thermal excitations, the intrinsic charge carrier concentration is zero, and graphene is consequently characterized as a zero-bandgap semiconductor. Notwithstanding the theoretical implications of this, practical and functioning graphene-based devices still require the existence of charge carriers, as well as control over the quantification of the concentrations and types of charge carriers (i.e., for *n*- or *p*-doping) [7, 8].

Intensive research performed over multiple decades into graphene material has further uncovered the remarkable chemical and material properties of this unique and somewhat extraordinary form of carbon. Perhaps most notably are the extremely high charge carrier mobilities in the range of 2000–5000 cm^2/V s, making graphene a choice material for implementation in high-speed electronics, such as flexible ultrafast microelectronics. Graphene is likewise one of the most highly conductive materials known with thermal conductivities reaching 5000 W/m K, facilitating its use for applications such as light-emitting diodes (LEDs).

Furthermore, having Young's modulus reportedly as high as 1 TPa has led to the use of graphene for strength reinforcement in various aerospace and structural/concrete material applications. In offering one of the largest specific surface areas (2630 m^2/g) combined with nearly full optical transparency of 97.7%, graphene has likewise been employed for the advancement of numerous optical and

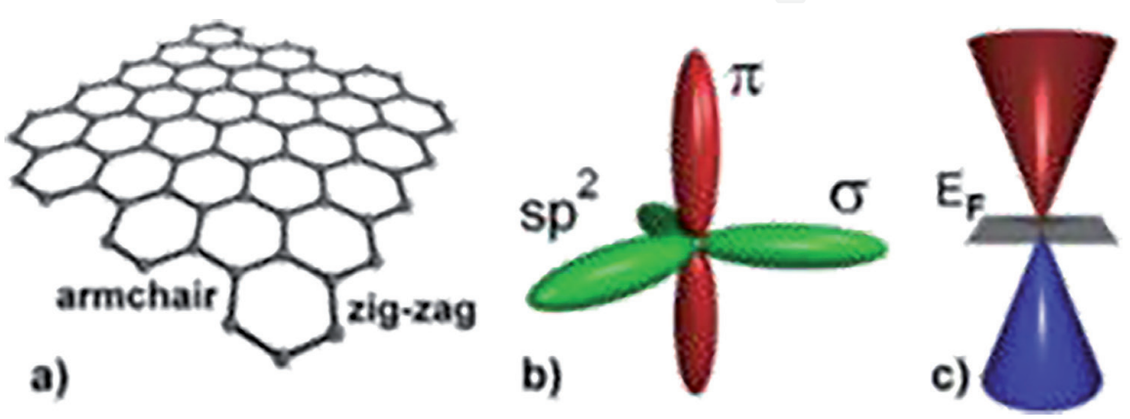

Figure 1.
(a) Graphene geometry; (b) bonding diagram; and (c) associated band diagram [5].

optoelectronic applications [9, 10]. The combined benefits of its high mechanical strength, optical transparency, and mobility of charge carriers have made graphene a choice material for a diverse array of electrical and/or optical applications.

During past decades, starting with the disclosure of the Hummers method in the 1950s followed by the chemical reduction of graphene oxides in 1962, there have been numerous research and studies on graphite oxide synthesis [8]. However, it took the work of A. Geim and K. Novoselov to fully isolate and subsequently characterize pristine graphene by a process of mechanical exfoliation that came to be known as the "Scotch tape" method for the properties of graphene to be more adequately understood, upon which it soon became a primary material of interest for many diverse ongoing research efforts. Later in 2010 Geim and Novoselov were awarded the Nobel Prize in Physics for this research encompassing graphene as a 2-D atomic structure [9].

After the initial success of isolating this graphitic material, many in the scientific community commenced to explore different processes and techniques for the large-scale synthesis and fabrication of graphene. As reported contemporarily in literature, the more common graphene synthesis processes included the oxidation-reduction growth process, chemical vapor deposition (CVD), liquid phase stripping, and epitaxial growth on silicon carbide (SiC) [10]. Among these various methods, the CVD process soon became the most established technique for producing graphene films with the highest quality crystalline and structural integrity, primarily on Cu substrates [11].

However, Cu and other metal substrates are not practical for most applications, as many optoelectronic-, sensor-, and microelectronics-based applications require the placement of graphene films directly on metal oxide or semiconductors. There, therefore, has been and remains a need for more optimized increasingly effective processes through which graphene films can be directly and effectively transferred onto any desired substrate of choice, while also avoiding cracks, wrinkles, and forms of contamination [12].

1.2 Graphene-based technological device development

Infrared detector and focal plane array (FPA) technologies are at the heart of many space-based instruments for NASA and defense missions that provide remote sensing and long-range imaging capabilities [13]. While often considered exotic in comparison to more established detector materials such as HgCdTe, on account of its gapless band structure, strong light-matter interaction, and the relative ease by which heterostructures may be fabricated, graphene can provide numerous capabilities from diverse means for effective broad spectra photodetection.

Graphene detector implementation can likewise further facilitate reduced size, weight, power, and cost (SWaP-C) mid-wave infrared (MWIR) sensors on smaller platforms, a high priority for providing improved measurement and mission capabilities in space. Use of process techniques such as post-growth thermal cycle annealing (TCA) has additionally been reported to enable up to an order of magnitude reduction in the dislocation density down to the saturation limit ($\sim 10^6$ cm^{-2}) for improved high-temperature operability of HgCdTe-on-Si-based MWIR detectors and FPAs [13].

The overall functionality and applicability of a detector device or system are governed primarily by its wavelength range, that is, band, of operation. Of the different infrared (IR) bands spanning the short-wave infrared (SWIR) to very long-wave infrared (VLWIR), the MWIR region is considered of the highest beneficial for long-range imaging and early threat detection [14]. Specifically, the 2–5 μm MWIR spectral band is crucial for NASA Earth Science applications, especially in

satellite-based LIDAR systems that require measuring a wide variety of natural features, including cloud aerosol properties, sea surface temperatures, and natural phenomena such as volcano and forest fires.

Though prior scientific reporting of associated experimental results has served to illuminate the key 2-D nanomaterial properties of graphene for enhancement of sensing performance particularly for IR band detection, certain challenges still must be addressed, which are as follows:

1. The existence of a process and technique for doping bilayer graphene with holes and electrons having sufficient charge carrier concentration. The main emphasis here is that the process of doping the graphene should not affect the crystalline structure and that the doped graphene film remains defect-free. This process should moreover be cost-effective and scalable for doping large-area graphene films.

2. The development of a method and process for transferring CVD-grown graphene to the desired substrate that ensures a uniform, clean, and intact transfer required for successful realization in an array of prospective applications.

3. Attainment of graphene-enhanced high mobilities and corresponding high level of photodetection performance in graphene-HgCdTe-based IR, and specificity 2–5 μm MWIR, photodetectors, and optical imaging arrays.

2. Graphene-enhanced MWIR photodetectors

2.1 Motives and objectives of device concept

HgCdTe, or MCT, the most widely used infrared (IR) detector material in military applications, is a direct energy bandgap semiconductor having a bandgap that is tunable from near-infrared (NIR) and SWIR to VLWIR bands through varying the Cd composition [15]. Typically, 0.3:0.7 Cd:Hg ratio results in a detectivity window over the SWIR to MWIR wavelength range.

Additionally, HgCdTe layer growth is highly controllable with certain deposition techniques. Notably among these is molecular-beam epitaxy (MBE), which yields high precision in the deposition of detector material structures leading to excellent control over optical excitation evidenced by the high quantum efficiencies (QE) demonstrated by HgCdTe-based detectors and sensors over the IR.

While adding considerable cost and bulk, cryogenic cooling is commonly utilized for IR detection to minimize thermally generated dark current. Since dark current increases with cutoff wavelength longevity, this requirement becomes even more important for MWIR and long-wave infrared (LWIR) sensors. IR band detector technologies that can operate at or near room temperature and substantially avoid costly and bulky cooling requirements, therefore, offer great practical benefits for many types of applications.

The incorporation of a high mobility graphene channel in HgCdTe-based detectors is a newly discovered means to offer further performance improvements and operational capabilities for MWIR detection. The intrinsic interfacial barrier between the HgCdTe-based absorber and the graphene layers thereby may be designed to effectively reduce the recombination of photogenerated carriers in the detector. The graphene thus functions as a high mobility channel that whisks away carriers before they can recombine, further contributing to the MWIR detection performance compared to in photodetectors only utilizing HgCdTe absorption layers [16].

2.2 Physical graphene-enhanced detector structure

The graphene-enhanced HgCdTe MWIR detector structure fabricated on a silicon substrate comprises three principal layers. First, a layer of CdTe is grown to act as a buffer layer functioning as the gate terminal (1). This layer provides an electrical field in the "vertical" direction into the detector heterostructure that aids in carrier transport in that direction. **Figure 2** shows a schematic of this detector structure as shown in a study by Srivastava et al. [12].

The HgCdTe absorber layer (2) is grown above the silicon substrate and the CdTe buffer layer acts as the active optical layer where photogeneration of carriers takes place. The HgCdTe absorber material and its physical properties, such as bandgap, determine the sensitivity of the absorber layer to the detection wavelength window. In addition, the absorber material governs the photogeneration rate, quantum efficiency, and carrier lifetime, which collectively contribute to overall detection performance.

Finally, the graphene layer (3) incorporates the role of high mobility, low noise channel that quickly whisks away the photogenerated carriers in the absorber into the contacts, and subsequently into the readout integrated circuit (ROIC) for electrical readout. This layer, therefore, is directly contacted to the ROIC.

2.3 Graphene-HgCdTe detector operating principle

The general operating principle of the graphene-HgCdTe MWIR photodetector may be described in terms of the life cycle of the photogenerated carriers [17]. Incident IR photons transmitted through the Si substrate and CdTe layers into the HgCdTe region are absorbed and produce electron-hole pairs, or excitons (**Figure 3**(**a**)). The vertical electric field in the absorber applied through modulation of the gate voltage effectively separates the electron-hole pairs due to the consequent opposing forces on electrons and holes. This separation of the carriers physically isolates the two photogenerated carrier species and suppresses the Auger recombination within the absorber, minimizing the loss of photogenerated carriers and is thus critical to the ultimate performance of the detector.

After separation, the carriers are transported through the absorber film toward the graphene interface and then injected into it (**Figure 3**(**b**)). Modulation of the gate voltage bias to preferentially inject only one of the photogenerated species into the graphene in a rectifier-like action enables dynamic control of the interface properties. As this process involves the injection of both species, it further prevents any Auger recombinations from taking place in the graphene.

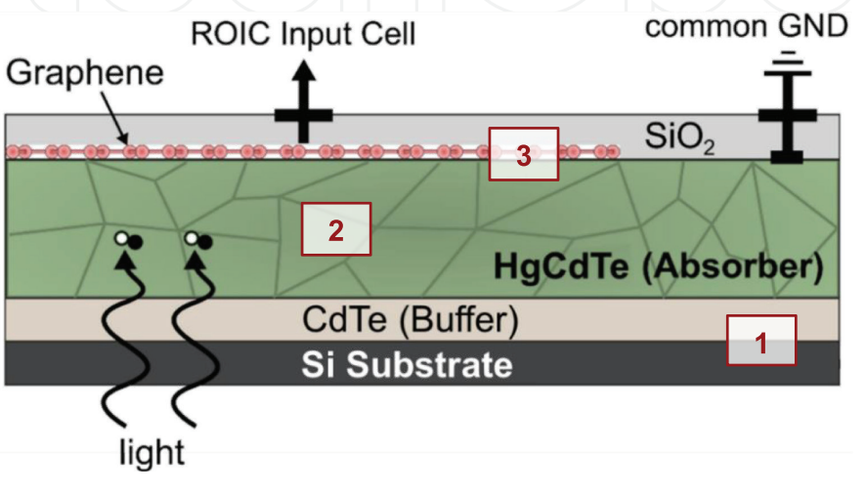

Figure 2.
Heterostructure layer structure of HgCdTe-graphene-based IR photodetector [12].

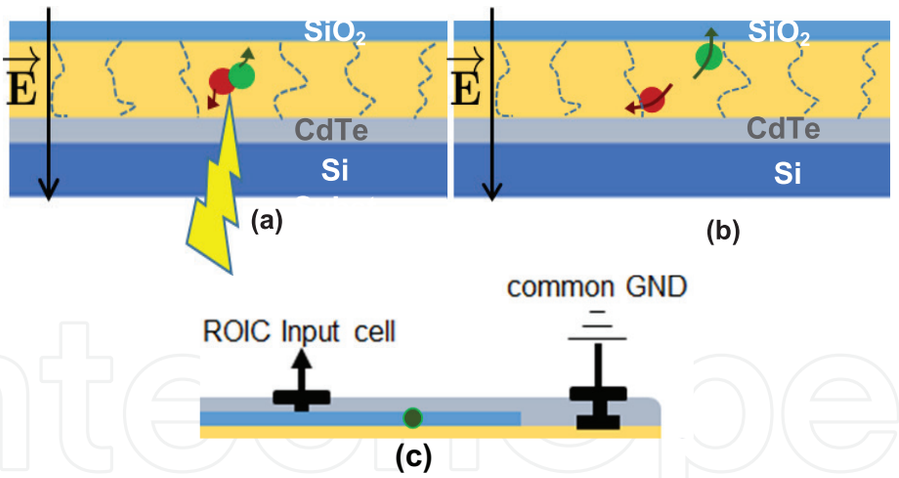

Figure 3.
(a) Generation of excitons from incident photons separation of electrons and holes due to applied gate electric field. (b) Photogenerated carrier transport and injection into graphene. (c) Horizontal transport of the photogenerated carriers in the graphene.

The carriers injected from the absorber into the graphene are transported laterally to the ROIC terminal and subsequently collected into it (**Figure 3**(**c**)). The establishment of a separate high mobility channel enabled by the graphene allows faster modulation frequencies with reduced **1/***f* noise and consequently higher performance metrics. Dynamic gating is additionally provided through the electrical control of carriers injected into the graphene.

3. Graphene-HgCdTe detector modeling effort

3.1 Modeling approach

The modeling effort was individually built upon various elements that combine to form a comprehensive model for this detector material technology. The overall goal of this modeling approach was to determine through simulations an accurate determination of electrical detector device behavior, including I-V characteristics, noise, responsivity, and other performance metrics. In addition, the directivity D* and noise equivalent temperature difference (NETD) may be derived from basic material parameters and device design and operating specifications to allow and guide further design optimizations.

The modeling effort, depicted schematically in **Figure 4**, entailed modular construction of the complete detector simulation platform from the individual models as data were made available from experiments and device characterizations. These have involved specific material modeling of the HgCdTe, graphene, and HgCdTe-graphene interface.

3.2 Modeled performance parameters in HgCdTe

This graphene-HgCdTe MWIR detector fundamentally functions as a photo-controlled current source rather than a light/heat-dependent resistance, characteristic of the typical operating mode for bolometers. **Figure 5** compares the theoretical dark current and photocurrent, film resistance, and detectivity (D*) performance parameters in the HgCdTe for a conventional photoconductive detector (**Figure 5**(**a**)) with that for this type of HgCdTe-based MWIR detector (**Figure 5**(**b**)). It is here noted that D* does not change appreciably because ultimately the material properties are

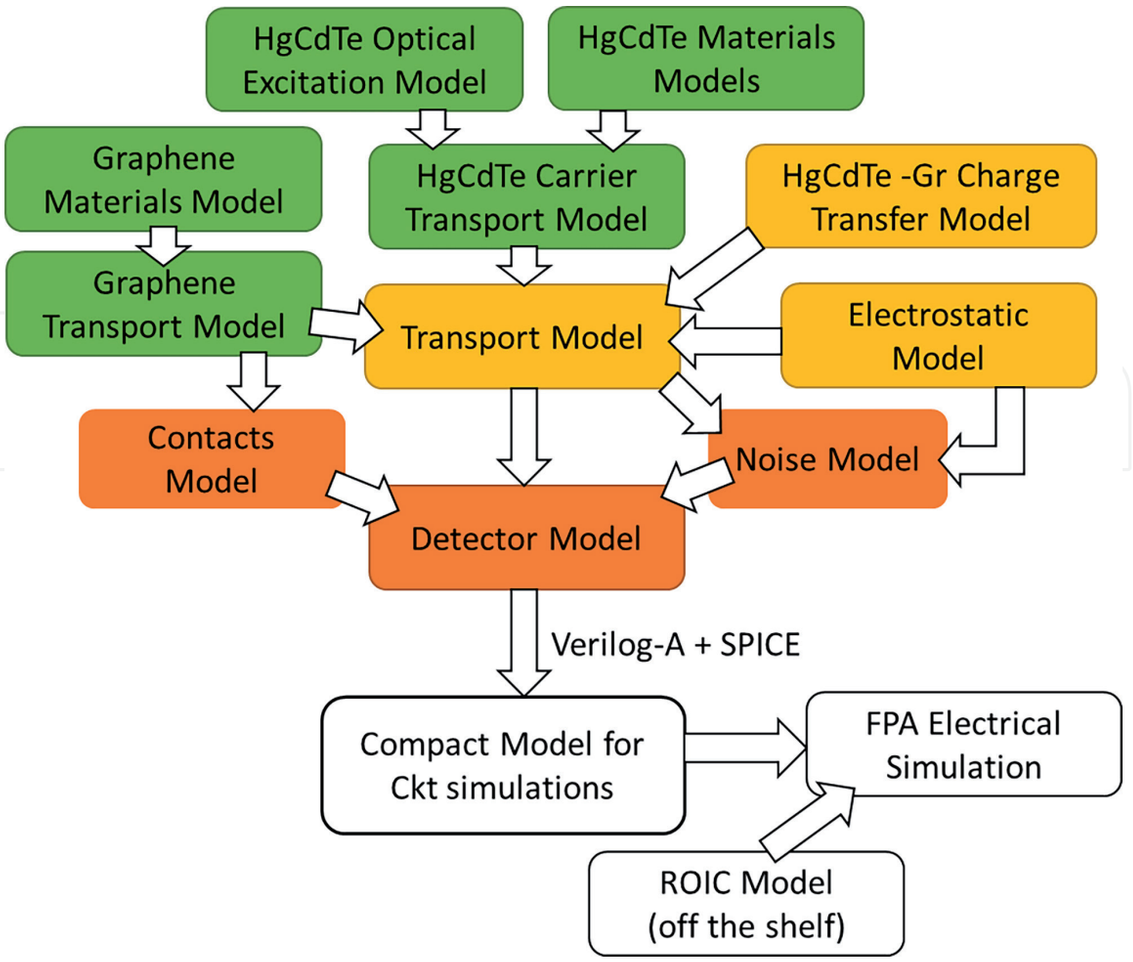

Figure 4.
Flowchart diagram illustrating the modeling approach and relationship between the different models utilized.

the same; altering the area of the current collection does not significantly change this fundamental property. The current and resistance, however, are each significantly lower for this latter detector design in view (**Figure 5**(**b**)). The incorporation of high mobility graphene in this detector can further enable higher responsivity and greater D*.

3.3 Graphene-HgCdTe interface band structure models

Figure 6 shows the *E-k* dispersion relation and density of states (DOS) determined for the HgCdTe/graphene interface. The contribution of individual atoms to the DOS is likewise computed. The carbon contributes maximally to the conduction band, while HgCdTe species contribute to the valence band.

Bandgap engineering of the HgCdTe detector material is additionally possible through adaptive control of the epitaxial growth process parameters. This provides the capability to optimize the performance to achieve desired spectral range and operating temperature specifications for the development of graphene-enhanced MWIR detectors and FPAs.

The work function of $Hg_{0.73}Cd_{0.27}Te$, ΦMCT, is determined (5.52 eV) based on the following relation:

$$\Phi_{MCT} = x\Phi_{\mathrm{CdTe}} + (1-x)\Phi_{\mathrm{HgTe}} \tag{1}$$

where x is the CdTe concentration in $Hg_{1-x}Cd_xTe$, and Φ_{CdTe} and Φ_{HgTe}, the work functions of CdTe and HgTe, are 4.5 eV and 5.9 eV, respectively. As shown in

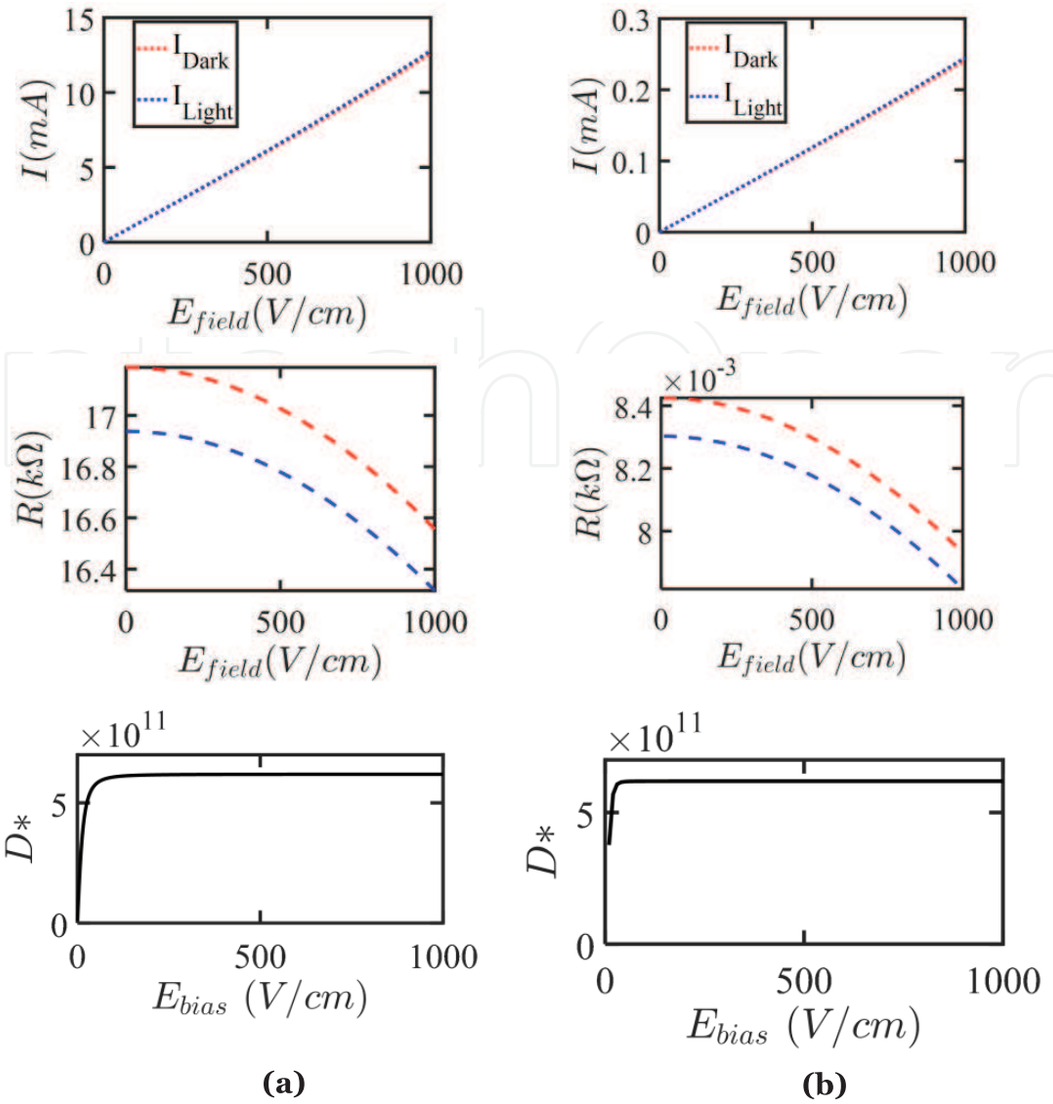

Figure 5.
Modeled dark current and photocurrent, film resistance, and detectivity (D) (from top to bottom) in HgCdTe for (a) conventional photoconductive detector design, and (b) design of this HgCdTe MWIR photoconductive detector.*

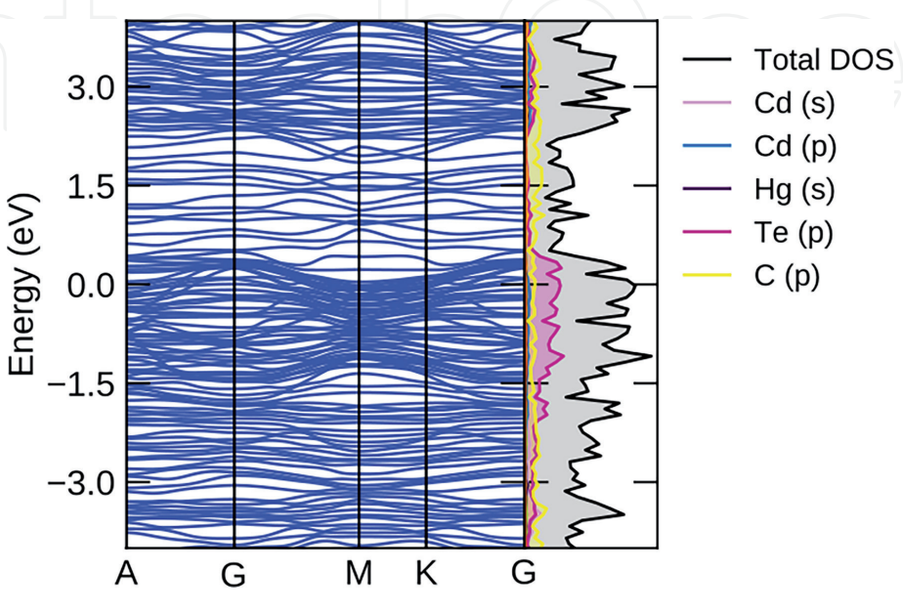

Figure 6.
E-k dispersion relation and density of states for HgCdTe/graphene interface.

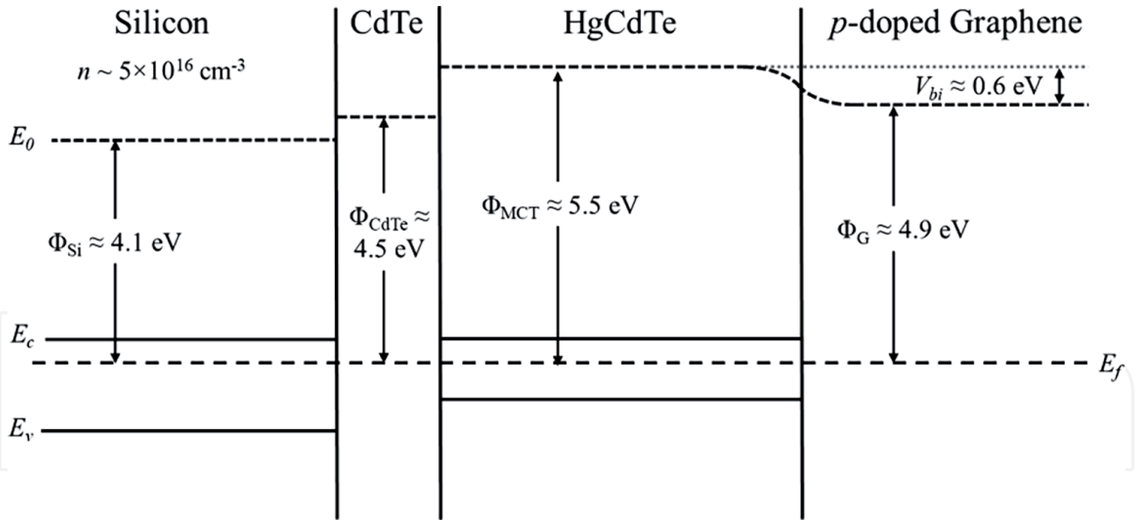

Figure 7.
Band diagram for graphene/HgCdTe/Si detector heterostructure.

Figure 7, $Hg_{0.7}Cd_{0.3}Te$ produces a built-in V_{bi} potential with *p*-doped graphene of ~0.6 eV. (With *n*-doped graphene having a work function 4.25, V_{bi} becomes as high as 1.27 eV.) Given its intermediate work function between that of HgCdTe (5.5 eV) and *n*-doped Si (4.1 eV), the use of the CdTe buffer layer facilitates band matching of the HgCdTe/CdTe/Si layers.

4. Doping of graphene bilayers

4.1 Historical development of graphene doping techniques

Recently a significant amount of research has been dedicated toward the manipulation of the physicochemical and electrical properties of graphene to specifically tailor it for various applications. One means to achieve this is through chemically functionalizing the graphene, involving modification of its carbon sp^2 honeycomb structure [18]. This chemical functionalization in turn necessitates chemically doping the atomic lattice of graphene with atoms from other compatible elements of the periodic table, essentially modifying graphene lattice originally undoped into a heteroatomically doped one.

The technique of doping through inducing charge carriers comprising either holes or electrons may be divided into two broad categories, which are as follows:

a. *Electrical doping*: In this process, charge carriers are induced by the application of an electric field. This can take place using a graphene-based field-effect transistor (FET), wherein the charge carriers are induced by an electric field produced by the gate structure. For example, with a Si^+/SiO_2 substrate varying the gate voltage V_g and consequently the concentration of electron/holes charge carriers enables the concentration of the induced carriers to be controlled by way of the applied gate voltage. If V_g is positive excitation of electrons and *n*-type doping will result, while on the other hand, an applied negative voltage will lead to induction of holes and a *p*-doped material. The concentration of charge carriers induced by this method can be as high as 10^{13} cm^{-2} [19].

b. *Chemical doping*: This technique involves the association of other chemical species with graphene and is further subdivided into two additional classifications, which are s*ubstitutional doping* and *surface transfer*. *Substitutional doping*

is a process whereby carbon atoms in the graphene lattice are substituted with other atoms, leading to either *p*-type or *n*-type conductivity [20]. Likewise, *surface transfer* describes a nondestructive technique for inducing charge carriers, in this case within the graphene lattice involving charge transfer between surface adsorbates and the graphene [21].

Doping by surface transfer may occur as the result of two different mechanisms—*electronical doping* and *electrochemical doping* [22]. Electronic doping is due to the direct transfer of charge between the graphene and adsorbate. In the presence of a differing electronic chemical potential, the doping type is controlled by the position of the graphene Fermi level relative to the highest occupied (HOMO) and lowest occupied (LUMO) level molecular orbitals of the adsorbate. While graphene is usually *n*-doped when the adsorbate HOMO lies above graphene Fermi level, *p*-type doping occurs when the LUMO of the adsorbate is found below the graphene Fermi levels [7]. The representation of molecular orbitals levels to the graphene Fermi levels for (a) *p*-type and (b) *n*-type doped graphene is shown in **Figure 8**. In contrast to electrical doping, electrochemical doping is a time-dependent process influenced by various factors that include the reaction rate and diffusion rate of molecular species [23].

The focus here is on inducing *p*-type doping in graphene through chemical doping. Chemical heteroatom doping of graphene is generally performed using either a one-step or two-step synthesis method. The one-step method involves employing CVD to introduce both carbon and boron sources into the chamber while heating the copper foil at high temperatures [24].

The alternative two-step synthesis process for boron doping includes thermal annealing [25] and rapid Wurtz-type reactive coupling [26] techniques, among others. Nevertheless, such two-step methods generally involve more complex experimental setups, tend to result in defects present in the doped graphene films, and require the use of toxic chemicals as the source/precursor as well as relatively high temperatures. These factors clearly limit the types of substrates that may be practically used [27].

However, a recently developed technique known as the spin-on dopant (SOD) process has made it possible to avoid these shortcomings in large part [28]. This

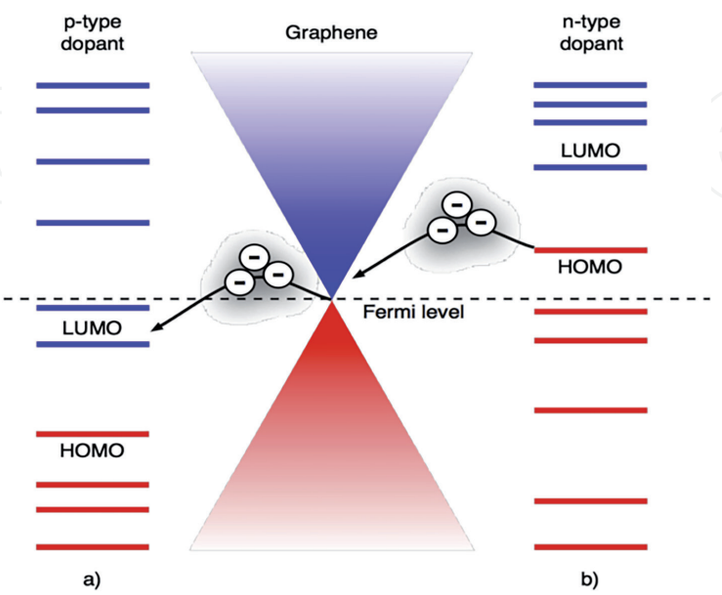

Figure 8.
Relative position of highest occupied (HOMO) and lowest unoccupied (LUMO) molecular orbitals of an adsorbate to the Fermi level of graphene for (a) p-type and (b) n-type dopants [6].

method, which we have adopted for producing *p*-type doping in graphene and shall subsequently be described in more comprehensive detail, requires only a relatively basic experimental setup without the need for toxic precursor gases.

4.2 Boron doping of bilayer graphene

Dopants used for chemically doping graphene include, but are not limited to, S, N, B, P, I, Se, O, and I [20, 21]. Among these dopant elements, the two most common and notable are nitrogen (N) and boron (B), for inducing *n*-type conductivity p^+-type conductivity, respectively, in graphene [22].

As the MWIR photodetector device under consideration requires *p*-doped graphene for optimal performance, the boron doping method is here in view. Boron is one of the most natural choices for doping among the atomic elements, having valence atoms that differ in number by only a single atom compared to the number of its carbon ones [29]. Atoms of boron also have a similar atomic size (0.088 nm atomic radius) to those of carbon (atomic radius of 0.077 nm), a factor that further facilitates *p*-type conduction in graphene [30].

When a dopant atom such as in this instance boron is bonded within a carbon framework, a defect is introduced into the neighboring site. Since boron only contains three valence electrons compared to four in carbon atoms, this can cause uneven charge distribution resulting in charge transfer between nearby carbon atoms, further expounding their electrochemical behavior [31]. The incorporation of a relatively small number of boron atoms thereby effectively lowers the Fermi level and formation of an acceptor level in the doped graphene. The introduction of boron likewise contributes to improved stabilization of the extremities of the graphene material and similarly aids in mitigating the termination of its layers, thereby promoting layer-by-layer growth of larger portions or sections of graphene [32].

4.3 Graphene spin-on doping process

We have developed and implemented a distinct spin-on dopant (SOD) process to produce highly boron-doped bilayer graphene. The SOD process involves spin-coating a dopant solution onto a source substrate and annealing the latter in conjunction with a target substrate in a tube furnace [31]. The bilayer graphene sheets doped using this process were deposited on SiO_2/Si substrates (300 nm SiO_2, *p*-type doped) by CVD acquired from Graphenea, Inc.

In the high-temperature environment and inert gas (e.g., argon) atmosphere, diffusion of the dopant (boron) from the source substrate into the target sample (bilayer graphene) occurs when the B atoms replace the C atoms to form *p*-doped graphene. The main advantages of this technique are its low cost and simplistic setup, combined with the capability to provide uniform and consistent doping profiles [33]. **Figure 9** depicts a schematic representation for substitutional doping of boron in the honeycomb lattice of graphene by the SOD process.

For the SOD procedure schematically illustrated in **Figure 9**, we start with the CVD-deposited graphene on Si/SiO_2 substrates. The spin-on diffusant used is Filmtronics B-155 (4% boron conc.). This boron source is spin-coated onto a Si wafer at 2300 rpm for 30 s using a CEE vacuum coater tool [34].

This boron-solution-coated source wafer is then placed in a custom-designed silica boat approximately 10 mm apart from and facing a target graphene sample. These are each inserted into a tube furnace that is pumped down to 10 Torr vacuum pressure and annealed in the presence of flowing Ar gas.

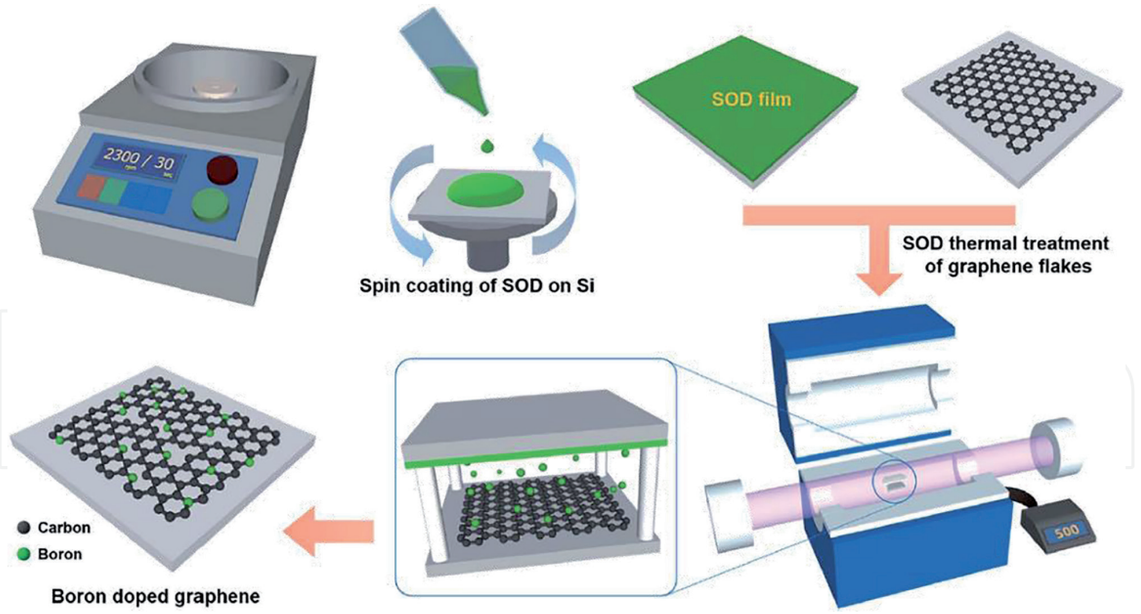

Figure 9.
Schematic of processing steps for the fabrication of boron-doped GFs through a spin-on dopant (SOD) method [32].

Parameter	Value
Temperature	500, 600°C
Flow gas	Argon
Flow rate	550 sccm
Ramp rate	15°C/min
Vacuum pressure	10 Torr
Boron source	Filmtronics B155 (4%)
Spin speed	2300 rpm
Spin time	30 s

Table 1.
Annealing and spin coating parameters for the SOD process.

Experimental parameters for the boron doping of graphene are given in **Table 1**. The goal of this process is to achieve required high doping levels while maintaining graphene surface features and quality for graphene-enhanced HgCdTe MWIR photodetectors.

4.4 Graphene boron-doping concentration analysis

To determine the structural properties, chemical bonding states, and doping concentration changes in the doped bilayer graphene, Raman spectroscopy and time-of-flight (ToF) secondary-ion mass spectroscopy (SIMS) techniques were performed as along with X-ray photoelectron spectroscopy (XPS).

Doping concentration vs. depth profile results for different boron-doped graphene bilayers using SIMS are presented in **Figure 10**. This graphene sample on Si/SiO_2 was doped with the SOD process using 15 min. Annealing duration. The SIMS analysis indicates boron doping levels of ~1.8×10^{20} cm^{-3} of boron in the graphene bilayers further confirmed by XPS.

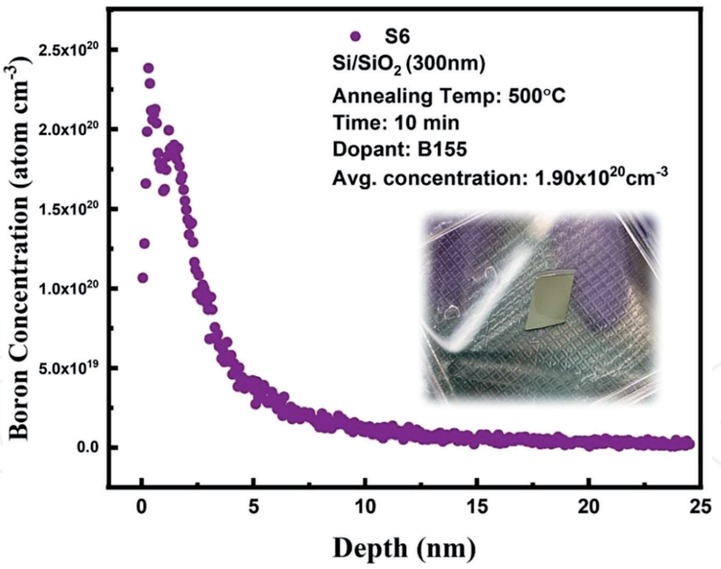

Figure 10.
SIMS atomic dopant concentrations vs. depth profiles for two different p-doped graphene samples on Si/SiO_2 substrates.

5. Substrate transfer of doped bilayer graphene

5.1 Evolution of substrate transfer techniques

Considerable research has been undertaken to synthesize graphene on metal substrates using the CVD process to produce high-quality large-area graphene films. Sufficiently high quality of graphene films is demonstrated by a single-crystalline structure free of wrinkles, contamination, and cracks [35]. However, various and often critical applications can require that the CVD-grown graphene films be transferred onto other more suitable substrates.

The earliest form of transfer for graphene can be traced back to the synthesis of graphene by "Scotch tape method," whereby graphene flakes were exfoliated and isolated from the graphite substrate onto another target substrate [34]. The development of an efficient process for transfer of graphene from its native substrate onto another foreign nevertheless has since proved relatively challenging, especially for large-area and intact graphene films [36].

While CVD-grown graphene on metal substrates is typically of high quality and purity, the deposited graphene when transferred off onto other types of substrates can easily degrade and suffer from contamination and structural damage [37]. Common sources of contamination during the process of graphene transfer include residues from the source substrate, etchant solutions used to dissolve the source substrates, and unwanted organic contamination due to the adherence of polymer compounds to the graphene following completion of the transfer [38]. These factors can lead to the formation of more charge carrier scattering centers that affect the electrical properties and mechanical stability of that graphene films, generally resulting in undesired doping of the graphene [39].

Additionally, the extreme thinness of graphene (single-layer atomic thickness for monolayer graphene) makes it inherently more vulnerable to altercation and impairment [40]. During cleaning and repeated transfer, mechanical strains can arise in the graphene that potentially can cause irreversible damage [41]. Hence, the need to maintain structural integrity and uniformity of the graphene for various applications can be very essential, for instance for optoelectronic devices or sensors

requiring charge injection between the active functional layer and highly pure and conductive graphene [42].

Furthermore, implementation of an optimized transfer process is critical to boost yield and reproducibility for low cost and scalable production of large-area graphene films [43]. Consequently, significant research is being undertaken to further optimize the process of transferring graphene to attain intact and dislocation- and defect-free graphene films.

The procedure required for preparing graphene for transfer may be characterized by the more relevant process steps involved, which typically include—(a) graphene layer removal from substrate utilizing liquid etchant, bubble transfer, or thermal peel off; (b) use of supportive layers (e.g., polymers such as PMMA and camphor) to prevent cracks, creases, and other structural damage; and (c) cleaning and removal/transfer of the grown layer from the substrate and protective layers [35].

The major graphene transfer methods reported in the literature are as follows:

a. *Bubble-mediated transfer*: In this process, H_2 and O_2 bubbles are produced due to electrochemical reactions, that is, by the graphene when CVD-grown on a metal substrate such as Cu/Ni acting as an electrode (either anode or cathode). These bubbles when generated apply a pealing-inducing force on the substrate surface, eventually leading to delamination of the graphene from the growth substrate.

Although this method is challenging in certain respects and more limited in that conductive substrates are necessary for the actualization of the electrode-initiated electrochemical reactions [30], considerable improvements have been discovered and incorporated over time. Goa et al. developed a nondestructive bubble-mediated transfer process that enabled repeated use of the growth (Pt) substrate, whereby the transferred graphene was found to have high carrier mobility along with minimal wrinkles [42]. Another study examined the use of PMMA/graphene/Cu acting as both an anode and cathode to remove a graphene sheet by bubble delamination, resulting in the reportedly high-quality transfer of the graphene films [40].

b. *Wet transfer*: This transfer method involves the use of ionic etchants to dissolve the growth substrate, after which the graphene is washed with a liquid cleaning agent and transferred to desired target substrate without drying [43]. The commonly used liquid etchant consists of ammonium persulfate aqueous solution and ferric chloride solution for dissolving Cu/Ni foil [44].

c. *Dry transfer*: While techniques for transferring graphene have traditionally relied on liquid etchants and cleaning solutions, this renders the growth substrates unusable consequently making these processes less economically viable. To circumvent in part these limitations, the dry transfer method was developed involving the incorporation of an inorganic metal oxide lifting layer (e.g., of MoO_3), which due to its low binding energy with the graphene films may be subsequently washed away completely. This process leads to high-quality graphene films without further contamination [45].

Through this experimentation toward the achievement of clean, smooth, and reduced-residue transfer, a PMMA-based resist-assisted transfer process was identified and established. In contrast to more conventional PMMA transfer processed known to leave residues during the graphene transfer, the method we have adapted

and further developed features a more straightforward process that uses different polymeric supportive layers for residue-free and clean transfer of graphene to avoid cleaning and support removal steps. This new method for transferring graphene from Si/SiO_2 to HgCdTe substrates combines both wet transfer and nonelectrochemical reaction-based transfer methods.

5.2 Experimental bilayer graphene transfer

Boron p^+ doping of bilayer graphene on Si/SiO_2 substrates has been accomplished to provide required electrical performance characteristics for a high mobility graphene channel in MWIR HgCdTe photodetector devices. The final step as discussed in this process involves transferring the sheets of highly p-doped bilayer graphene from the original Si/SiO_2 onto HgCdTe substrates for incorporation in the MWIR photodetector and FPA devices. This subsequently p-doped bilayer graphene on Si/SiO_2 is transferred using a PMMA-assisted wet transfer process [44]. **Figure 11** shows schematically this experimental procedure for transferring the graphene onto HgCdTe [18].

Through this relatively straightforward procedure, the successful transfer of doped bilayer graphene sheets deposited on SiO_2/Si onto HgCdTe has been demonstrated. The graphene bilayers are preserved, and no morphological changes were observed, following the transfer process with their relocation where the spatial configurations of the bilayers were maintained across macroscopic regions.

5.3 Characterization of graphene transferred onto HgCdTe

Following the transfer of the p-doped graphene onto HgCdTe substrates, the doped bilayer graphene on HgCdTe was measured using optical microscopy and Raman spectroscopy to determine if any significant changes had occurred in its properties through the process. **Figure 12** presents optical microscopy images of

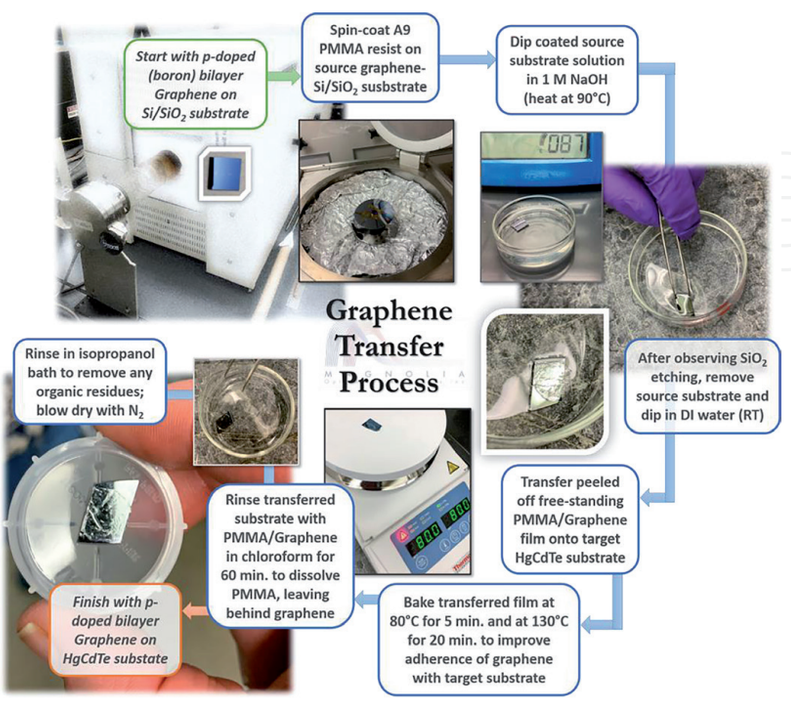

Figure 11.
Schematic outline of the experimental process enabling the removable transfer of bilayer graphene from SiO_2/Si onto HgCdTe substrates.

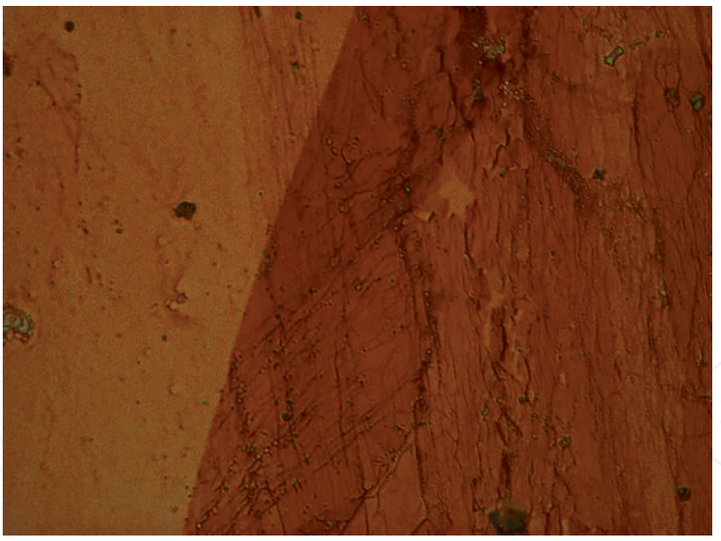

Figure 12.
Optical microscopy image of graphene deposited on HgCdTe, where darker areas represent graphene on HgCdTe and lighter area portions the bare HgCdTe substrate.

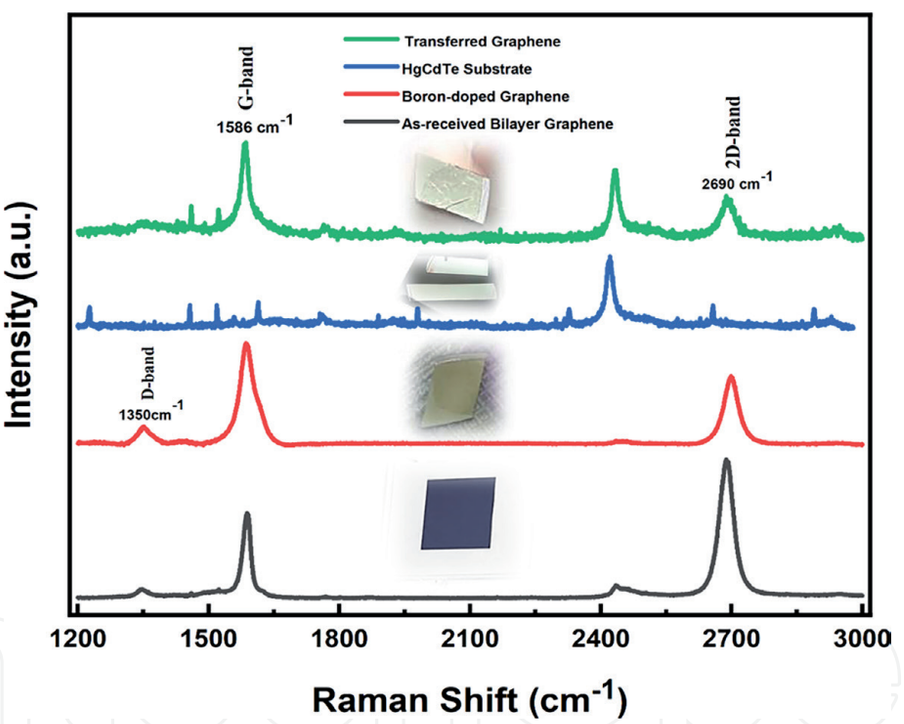

Figure 13.
Raman spectroscopy analysis of boron-doped graphene transferred onto HgCdTe substrate, compared to spectra of bare HgCdTe substrate, that of the pristine bilayer graphene on Si/SiO_2, and the graphene on Si/SiO_2 following the boron doping but before transfer.

the transferred graphene onto HgCdTe. The darker areas represent the part of the HgCdTe covered with graphene (having relatively marginal but practically observable differences in optical absorption), while the lighter areas indicate uncovered portions of the bare HgCdTe substrate.

Figure 13 shows Raman spectra of the transferred doped graphene on HgCdTe, in comparison to the as-received graphene on Si/SiO_2; the graphene following the boron doping; and a bare HgCdTe substrate.

The Raman spectroscopy analysis shows the G-band peak resulting from in-plane vibrations of sp^2-bonded carbon atoms, and the D-band peak due to out-of-plane vibrations attributed to the presence of structural defects. The associated

D/G ratio relates to the sp^3/sp^2 carbon ratio. The 2D-band, the second order of the D-band, is the result of a two-phonon lattice vibrational process.

The ratio of 2D/G intensities provides insight into the properties of the graphene layers. For example, a 2D/G band ratio in this case found in the range of 1–2 indicates a bilayer graphene structure. In addition, the same D-band and 2G-band graphene peaks present in the bilayer graphene prior to doping as well as in graphene samples doped on Si/SiO_2 have likewise observed in graphene transferred onto the HgCdTe substrate, thus demonstrating preservation of the structural integrity in the transferred bilayers of doped graphene.

6. Conclusions

The material and electrical properties of high-performance graphene-HgCdTe detector technology, where the graphene layer functions as a high mobility channel, developed for MWIR sensing and imaging for NASA Earth Science applications have been assessed. Comprehensive modeling of HgCdTe, graphene, and the HgCdTe-graphene interface has aided in the design and development of this MWIR detector technology.

By using a SOD process, we have achieved boron doping of the bilayer graphene. SIMS, XPS, and Raman spectroscopy-based characterization of the doping levels and properties have confirmed higher boron doping concentrations $>10^{20}$ cm^{-3} in the graphene layers. The *p*-doped graphene bilayers originally on Si/SiO_2 substrates have been furthermore transferred onto HgCdTe substrates, and the structural integrity of the transferred doped layers confirmed through various methods of characterization for implementation as high mobility channels in uncooled MWIR graphene-enhanced HgCdTe detection devices.

Successful integration of enhanced graphene into HgCdTe photodetectors can thereby provide higher MWIR detector performance as compared to HgCdTe detectors alone. Combined with the room temperature operational capability of the graphene-HgCdTe detectors and arrays, the fulfillment of the objective of attaining new earth observation measurement capabilities is a step closer to benefit and advancing critical NASA Earth Science applications.

Acknowledgements

This research is and has been funded by the National Aeronautics and Space Administration (NASA), Contract No. 80NSSC18C0024. The views and conclusions contained in this document are those of the authors and should not be interpreted as representing the official policies, either express or implied, of NASA or the U.S. Government.

Author details

Ashok K. Sood[1,2*], John W. Zeller[1,2], Parminder Ghuman[3], Sachidananda Babu[3], Nibir K. Dhar[4], Randy N. Jacobs[5], Latika S. Chaudhary[6], Harry Efstathiadis[6], Samiran Ganguly[7], Avik W. Ghosh[7], Sheikh Ziauddin Ahmed[7] and Farjana Ferdous Tonni[7]

1 Magnolia Optical Technologies, Inc., Woburn, MA, United States

2 Magnolia Optical Technologies Inc., Albany, NY, United States

3 NASA Earth Science Technology Office, Greenbelt, MD, USA

4 Department of Electrical and Computer Engineering, Virginia Commonwealth University, Richmond, VA, USA

5 U.S. Army Night Vision and Electronic Sensors Directorate, Fort Belvoir, VA, USA

6 College of Nanoscale Science and Engineering, State University of New York Polytechnic Institute, Albany, NY, USA

7 Department of Electrical and Computer Engineering, University of Virginia, Charlottesville, VA, USA

*Address all correspondence to: aksood@magnoliaoptical.com

References

[1] Zhang X, Rajaraman BR, Liu H, Ramakrishna S. Graphene's potential in materials science and engineering. RSC Advances. 2014;**4**:28987-29011. DOI: 10.1039/C4RA02817A

[2] Pham VP. Direct Growth of Graphene on Flexible Substrates Towards Flexible Electronics: A Promising Perspective. London: IntechOpen; 2018. DOI: 10.5772/intechopen.73171

[3] Jariwala D, Srivastava A, Ajayan PM. Graphene synthesis and band gap opening. Journal of Nanoscience and Nanotechnology. 2011;**11**:6621-6641. DOI: 10.1166/jnn.2011.5001

[4] Randviir EP, Brownson DA, Banks CE. A decade of graphene research: Production, applications and outlook. Materials Today. 2014;**17**:426-432. DOI: 10.1016/j.mattod.2014.06.001

[5] Sood AK, Lund I, Puri YR, Efstathiadis H, Haldar P, Dhar NK, et al. Review of graphene technology and its applications for electronic devices. In: Farzad Ebrahimi F, editor. Graphene—New Trends and Developments. London: IntechOpen; 2015. pp. 59-89. DOI: 10.5772/61316

[6] Pinto H, Markevich A. Electronic and electrochemical doping of graphene by surface adsorbates. Beilstein Journal of Nanotechnology. 2014;**5**:1842-1848. DOI: 10.3762/bjnano.5.195

[7] Novoselov KS, Jiang D, Schedin F, Booth TJ, Khotkevich VV, Morozov SV, et al. Two-dimensional atomic crystals. Proceedings of the National Academy of Sciences. 2005;**102**:10451-10453. DOI: 10.1073/pnas.0502848102

[8] Novoselov KS, Fal VI, Colombo L, Gellert PR, Schwab MG, Kim K. A roadmap for graphene. Nature. 2012;**490**:192-200. DOI: 10.1038/nature11458

[9] Geim A, Novoselov K. The rise of graphene. Nature Materials. 2007;**6**: 183-191. DOI: 10.1038/nmat1849

[10] Zhu Y, Murali S, Cai W, Li X, Suk JW, Potts JR, et al. Graphene and graphene oxide: Synthesis, properties, and applications. Advanced Materials. 2010;**22**:3906-3924. DOI: 10.1002/adma.201001068

[11] Dasari BL, Nouri JM, Brabazon D, Naher S. Graphene and derivatives—Synthesis techniques, properties and their energy applications. Energy. 2017;**140**:766-768. DOI: 10.1016/j.energy.2017.08.048

[12] Srivastava S, Jain SK, Gupta G, Senguttuvan TD, Gupta BK. Boron-doped few-layer graphene nanosheet gas sensor for enhanced ammonia sensing at room temperature. RSC Advances. 2020;**10**:1007-1014. DOI: 10.1039/C9RA08707A

[13] Sood AK, Zeller JW, Ghuman P, Babu S, Dhar NK, Jacobs R, et al. Development of high-performance graphene-HgCdTe detector technology for mid-wave infrared applications. In: Proceedings of SPIE. Vol. 11831. Bellingham: SPIE; 2021. p. 1183103

[14] Jacobs RN, Benson JD, Stoltz AJ, Almeida LA, Farrell S, Brill G, et al. Analysis of thermal cycle-induced dislocation reduction in HgCdTe/CdTe/Si(211) by scanning transmission electron microscopy. Journal of Crystal Growth. 2013;**366**:88-94. DOI: 10.1016/j.jcrysgro.2012.12.007

[15] Sood AK, Zeller JW, Pethuraja GG, Welser RE, Dhar NK, Wijewarnasuriya PS. Nanostructure technology for EO/IR detector applications. In: Ghamsari MS, Dhara S, editors. Nanorods and Nanocomposites. London: IntechOpen; 2019. pp. 69-93. DOI: 10.5772/intechopen.85741

[16] Dhar NK, Dat R, Sood AK. Advances in infrared detector array technology. In: Pyshkin SL, Ballato JM, editors. Optoelectronics—Advanced Materials and Devices. London: IntechOpen; 2013. pp. 165-208. DOI: 10.5772/51665

[17] Sood AK, Zeller JW, Ghuman P, Babu S, Dhar NK. Development of high-performance detector technology for UV and IR applications. In: IGARSS 2019-2019 IEEE International Geoscience and Remote Sensing Symposium; Yokohama; 28 July-2 August 2019. New York: IEEE; 2019. p. 20200000463

[18] Sood AK, Zeller JW, Ghuman P, Babu S, Dhar NK, Jacobs R, et al. Development of high-performance graphene-HgCdTe detector technology for mid-wave infrared applications. In: Proceedings of SPIE. Vol. 11723. Bellingham: SPIE; 2021. p. 117230I

[19] Agnoli S, Favaro M. Doping graphene with boron: A review of synthesis methods, physicochemical characterization, and emerging applications. Journal of Materials Chemistry A. 2016;**4**:5002-5025. DOI: 10.1039/C5TA10599D

[20] Bae S, Kim H, Lee Y, Xu X, Park JS, Zheng Y, Balakrishnan J, et al. Roll-to-roll production of 30-inch graphene films for transparent electrodes. Nature Nanotechnology. 2020;**5**:574-578. DOI: 10.1038/nnano.2010.132

[21] Mousavi H, Moradian R. Nitrogen and boron doping effects on the electrical conductivity of graphene and nanotube. Solid State Sciences. 2011;**13**:1459-1464. DOI: 10.1016/j.solidstatesciences.2011.03.008

[22] Yu X, Han P, Wei Z, Huang L, Gu Z, Peng S, et al. Boron-doped graphene for electrocatalytic N_2 reduction. Joule. 2018;**2**:1610-1622. DOI: 10.1016/j.joule.2018.06.007

[23] Nankya R, Lee J, Opar DO, Jung H. Electrochemical behavior of boron-doped mesoporous graphene depending on its boron configuration. Applied Surface Science. 2019;**489**:552-559. DOI: 10.1016/j.apsusc.2019.06.015

[24] Tennyson WD, Tian M, Papandrew AB, Rouleau CM, Puretzky AA, Sneed BT, et al. Bottom up synthesis of boron-doped graphene for stable intermediate temperature fuel cell electrodes. Carbon. 2017;**123**:605-615. DOI: 10.1016/j.carbon.2017.08.002

[25] Panchakarla LS, Subrahmanyam KS, Saha SK, Govindaraj A, Krishnamurthy HR, Waghmare UV, et al. Synthesis, structure, and properties of boron-and nitrogen-doped graphene. Advanced Materials. 2009;**21**:4726-4730. DOI: 10.1002/adma.200901285

[26] Fujisawa K, Hayashi T, Endo M, Terrones M, Kim JH, Kim YA. Effect of boron doping on the electrical conductivity of metallicity-separated single-walled carbon nanotubes. Nanoscale. 2018;**10**:12723-12733. DOI: 10.1039/C8NR02323A

[27] Feng L, Qin Z, Huang Y, Peng K, Wang F, Yan Y, et al. Boron-, sulfur-, and phosphorus-doped graphene for environmental applications. Science of the Total Environment. 2020;**698**: 134239. DOI: 10.1016/j.scitotenv.2019.134239

[28] Santhosh R, Raman SS, Krishna SM, Sai Ravuri S, Sandhya V, Ghosh S, et al. Heteroatom doped graphene based hybrid electrode materials for supercapacitor applications. Electrochimica Acta. 2018;**276**:284-292. DOI: 10.1016/j.electacta.2018.04.142

[29] Usachov DY, Fedorov AV, Vilkov OY, Petukhov AE, Rybkin AG, Ernst A, et al. Large-scale sublattice asymmetry in pure and boron-doped graphene. Nano Letters. 2016;**16**:4535-4543. DOI: 10.1021/acs.nanolett.6b0179

[30] Sin DY, Park IK, Ahn HJ. Enhanced electrochemical performance of phosphorus incorporated carbon nanofibers by the spin-on dopant method. RSC Advances. 2016;**6**:58823-58830. DOI: 10.1039/C6RA06782D

[31] Wu Y, Han Z, Younas W, Zhu Y, Ma X, Cao C. P-Type boron-doped monolayer graphene with tunable bandgap for enhanced photocatalytic H_2 evolution under visible-light irradiation. ChemCatChem. 2019;**11**:5145-5153. DOI: 10.1002/cctc.201901258

[32] Sahoo M, Sreena KP, Vinayan BP, Ramaprabhu S. Green synthesis of boron doped graphene and its application as high performance anode material in Li ion battery. Materials Research Bulletin. 2015;**61**:383-930. DOI: 10.1016/j.materresbull.2014.10.049

[33] Ren S, Rong P, Yu Q. Preparations, properties and applications of graphene in functional devices: A concise review. Ceramics International. 2018;**44**:11940-11955. DOI: 10.1016/j.ceramint.2018.04.089

[34] Jang AR, Lee YW, Lee SS, Hong J, Beak SH, Pak S, et al. Electrochemical and electrocatalytic reaction characteristics of boron-incorporated graphene via a simple spin-on dopant process. Journal of Materials Chemistry A. 2018;**6**:7351-7356. DOI: 10.1039/C7TA09517A

[35] Zagozdzon-Wosik W, Grabiec PB, Lux G. Silicon doping from phosphorus spin-on dopant sources in proximity rapid thermal diffusion. Journal of Applied Physics. 1994;**75**:337-344. DOI: 10.1063/1.355855

[36] Lee HC, Liu WW, Chai SP, Mohamed AR, Aziz A, Khe CS, et al. Review of the synthesis, transfer, characterization and growth mechanisms of single and multilayer graphene. RSC Advances. 2017;**7**:15644-15693. DOI: 10.1039/C7RA00392G

[37] Chen Y, Gong XL, Gai JG. Progress and challenges in transfer of large-area graphene films. Advanced Science. 2016;**3**:1500343. DOI: 10.1002/advs.201500343

[38] Kang S, Yoon T, Kim S, Kim TS. Role of crack deflection on rate dependent mechanical transfer of multilayer graphene and its application to transparent electrodes. ACS Applied Nano Materials. 2019;**2**:1980-1985. DOI: 10.1021/acsanm.9b00014

[39] Ullah S, Yang X, Ta HQ, Hasan M, Bachmatiuk A, Tokarska K, et al. Graphene transfer methods: A review. Nano Research. 2021;**5**:1-7. DOI: 10.1007/s12274-021-3345-8

[40] Ma LP, Ren W, Cheng HM. Transfer methods of graphene from metal substrates: A review. Small Methods. 2019;**3**:1900049. DOI: 10.1002/smtd.201900049

[41] Kostogrud IA, Boyko EV, Smovzh DV. The main sources of graphene damage at transfer from copper to PET/EVA polymer. Materials Chemistry and Physics. 2018;**219**:67-73. DOI: 10.1016/j.matchemphys.2018.08.001

[42] Gao L, Ren W, Xu H, Jin L, Wang Z, Ma T, et al. Repeated growth and bubbling transfer of graphene with millimetre-size single-crystal grains using platinum. Nature Communications. 2012;**3**:1-7. DOI: 10.1038/ncomms1702

[43] Leong WS, Wang H, Yeo J, Martin-Martinez FJ, Zubair A, Shen PC, et al. Paraffin-enabled graphene transfer. Nature Communications. 2019;**10**:1-8. DOI: 10.1038/s41467-019-08813-x

[44] Gorantla S, Bachmatiuk A, Hwang J, Alsalman HA, Kwak JY, Seyller T, et al. A universal transfer route for graphene.

Nanoscale. 2014;**6**:889-896.
DOI: 10.1039/C3NR04739C

[45] Park H, Lim C, Lee CJ, Kang J, Kim J, Choi M, et al. Optimized poly (methyl methacrylate)-mediated graphene-transfer process for fabrication of high-quality graphene layer. Nanotechnology. 2018;**29**(41): 415303. DOI: 10.1088/1361-6528/aad4d9